Bioorganic Chemistry 85 (2019) 97–108

Contents lists available at ScienceDirect

Bioorganic Chemistry

journal homepage: www.elsevier.com/locate/bioorg

In vitro and *in silico* evaluation of new thiazole compounds as monoamine oxidase inhibitors

Begüm Nurpelin Sağlık[a,b,*], Betül Kaya Çavuşoğlu[a], Derya Osmaniye[a,b], Serkan Levent[a,b], Ulviye Acar Çevik[a,b], Sinem Ilgın[c], Yusuf Özkay[a,b], Zafer Asım Kaplancıklı[a], Yusuf Öztürk[d]

[a] Department of Pharmaceutical Chemistry, Faculty of Pharmacy, Anadolu University, Eskişehir, Turkey
[b] Doping and Narcotic Compounds Analysis Laboratory, Faculty of Pharmacy, Anadolu University, Eskişehir, Turkey
[c] Department of Pharmaceutical Toxicology, Faculty of Pharmacy, Anadolu University, Eskişehir, Turkey
[d] Department of Pharmacology, Faculty of Pharmacy, Anadolu University, Eskişehir, Turkey

ARTICLE INFO

Keywords:
Thiazole derivatives
MAO inhibitors
Enzyme inhibitor activity
Molecular docking

ABSTRACT

New twenty compounds bearing thiazole ring (**3a-3t**) were designed and synthesized as monoamine oxidase (MAO) inhibitors. The fluorometric enzyme inhibition assay was used to determine the biological effects of synthesized compounds. Most of them showed remarkable inhibitory activity against both MAO-A and MAO-B. By comparing their IC_{50} values, it can be seen that active derivatives displayed generally selectivity on MAO-B enzyme. Compounds **3j** and **3t**, which bear dihydroxy moiety at the 3rd and 4th position of phenyl ring, were the most active derivatives in the series against both isoenzymes. Compounds **3j** and **3t** showed significant inhibition profile on MAO-A with the IC_{50} values of 0.134 ± 0.004 μM and 0.123 ± 0.005 μM, respectively, while they performed selectivity against MAO-B with the IC_{50} values of 0.027 ± 0.001 μM and 0.025 ± 0.001 μM, respectively. Also, docking studies about these compounds were carried out to evaluate their binding modes on the active regions of MAO-A and MAO-B.

1. Introduction

Monoamine Oxidases (MAOs) are flavin adenine dinucleotide (FAD) based enzymes being responsible for the catalysis of oxidative deamination of biological amines in both peripheral tissues and central nervous system (CNS). Two different types of MAOs are known as MAO-A and MAO-B. Both of them are placed to the mitochondrial membrane in neural, glial and some other tissues as integral proteins [1]. MAO-A consists of 527 amino acids, while MAO-B contains 520 amino acids. Their amino acid sequences have 70% similarity. MAO-A crystallizes as a monomer, whereas MAO-B exists as dimers. Specificities of MAO-A and MAO-B cause minor differences in the active sites [2–4]. The volume of the MAO-A active site is ~400 Å while the MAO-B active has ~700 Å volume [4–6]. Although both of two isoenzymes have substrate-binding cavity, their substrate selectivity is quite different. Inhibition of norepinephrine and serotonin was carried out by MAO-A, whereas inhibition of phenyl ethylamine and benzyl amine is carried out by MAO-B. Both enzymes are able to oxidize dopamine and tyramine. However, dopamine and tyramine are efficiently oxidized by MAO-A and MAO-B, respectively [7–10].

A healthy nervous system is one of the most valuable properties that a person has got. However, some disorders in the nervous system as depression, Parkinson's disease (PD) and Alzheimer's disease (AD) may affect the life of human. These disorders have been studied extensively and numerous drugs have been improved up to day [1,5,11–13]. MAO inhibitors are one of the promising choices in the treatment of these disorders. The increasing functional and structural information about MAO enzyme help to create better selective and reversible inhibitors. Current studies are targeting MAO-B for the treatment of PD and AD via generating the selective MAO-B inhibitors, while selective MAO-A inhibitors are important for the treatment of depression [14–16].

In the literature there are many thiazole compounds found to be effective against MAO enzymes. Among them the compounds bearing arylidene-hydrazinyl-thiazole substructure were reported to inhibit MAO enzymes, significantly [17–19] (Fig. 1). The SARs of previously reported hydrazinyl-thiazole compounds have clearly suggested the required structural features for a compound to possess enzyme inhibitory activity [20–27]. Prompted from the SARs data of these studies we recently performed a study including the MAO inhibitory activity of some benzylidene-hydrazinyl-thiazoles. [28]. Results of such study directed us to design and synthesize similar compounds for enhancing the MAO inhibitory activity. Hence, in the present study new benzylidene-

* Corresponding author at: Anadolu University, Faculty of Pharmacy, Department of Pharmaceutical Chemistry, 26470 Eskişehir, Turkey.
E-mail address: bnsaglik@anadolu.edu.tr (B.N. Sağlık).

https://doi.org/10.1016/j.bioorg.2018.12.019
Received 24 October 2018; Received in revised form 11 December 2018; Accepted 12 December 2018
Available online 13 December 2018

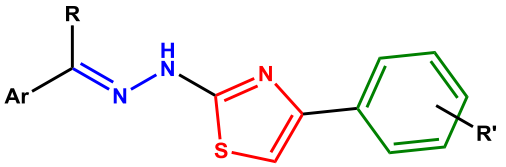

Fig. 1. General chemical structure of 2-[2-(Arylidene)hydrazinyl]-4-substitutedphenylthiazoles as MAO inhibitors. **Ar:** phenyl, pyridin-2-yl, pyridin-3-yl, pyridin-4-yl, naphthalen-1-yl, naphthalen-2-yl **R:** H, CH_3 **Ŕ:** 4-F, 4-CN were reported in previous studies [17–27]; **Ar:** 4-(Morpholin-4-yl)/(pyrrolidin-1-yl) phenyl **R:**H, **Ŕ:** H, 4-CH_3, 4-CN, 4-Br, 4-CI, 4-F, 2,4-DiCI, 2,4-DiF were reported in our recent study [28]; **Ar:** 4-(3- or 4-methylpiperidin-1-yl)phenyl **R:** H, **Ŕ:** H, 4-CH_3, 4-Br, 4-CI, 4-F, 4-NO_2, 4-CN, 4-OH, 2,4-DiF, 3,4-DiOH were synthesized in this study.

hydrazinyl-thiazoles were synthesized and tested for their MAO inhibition potency both in *in vitro* and *in silico* assays.

2. Materials and methods

2.1. Chemistry

All chemicals were purchased from Sigma-Aldrich Chemical Co (Sigma-Aldrich Corp., St. Louis, MO, USA) and Merck Chemicals (Merck KGaA, Darmstadt, Germany). All melting points (m.p.) were determined by MP90 digital melting point apparatus (Mettler Toledo, Ohio, USA) and were uncorrected. All reactions were monitored by thin-layer chromatography (TLC) using Silica Gel 60 F254 TLC plates (Merck KGaA, Darmstadt, Germany). Spectroscopic data were recorded with the following instruments: ^{1}H NMR, Bruker DPX 300 NMR spectrometer; ^{13}C NMR Bruker DPX 75 NMR spectrometer (Bruker Bioscience, Billerica, MA, USA) in DMSO-d_6, using TMS as internal standard; The IR spectra were recorded by an IRAffinity-1S Fourier transform IR (FTIR) spectrometer (Shimadzu, Tokyo, Japan). M + 1 peaks were determined by Shimadzu LC/MS IT-TOF system (Shimadzu, Tokyo, Japan).

2.1.1. General procedure for synthesis of 4-(3/4-methylpiperidin-1-yl) benzaldehydes (1a, 1b)

To a solution of 3- or 4-methylpiperidine (3.4 g, 0.034 mol) in DMF (10 mL) was added 4-fluorobenzaldehyde (4.3 g, 0.034 mol) and K_2CO_3 (4.7 g, 0.034 mol) then the reaction mixture stirred under reflux for 24 h. After cooling to the ambient temperature, the reaction mixture was poured into ice-water. The obtained solid was filtered off, washed with water and crystallized from ethanol to afford compounds **1a**, **1b**.

2.1.2. General procedure for synthesis of 2-(4-(3- or 4-methylpiperidin-1-yl)benzylidene)hydrazine-1-carbothioamides (2a, 2b)

A mixture of compounds **1a** or **1b** (5 g, 25 mmol), and thiosemicarbazide (2.3 g, 25 mmol) were refluxed in ethanol for 4 h. When the reaction was completed as indicated by TLC, the reaction mixture was cooled to attain room temperature. The precipitated product was filtered and recrystallized from ethanol to give **2a**, **2b**.

2.1.3. General procedure for synthesis of 2-[2-(4-(3- or 4-methylpiperidin-1-yl)benzylidene) hydrazinyl]-4-(substituted or disubstituted phenyl) thiazole derivatives (3a-3 t)

The target compounds (**3a-3 t**) were synthesized via the reaction of corresponding thiosemicarbazone (**2a, 2b**) (0.55 g, 2 mmol) and appropriate phenacyl bromide derivatives (2 mmol) in ethanol (40 mL) under reflux for 3 h. The mixture was cooled, precipitated product was collected by filtration, dried and recrystallized from ethanol.

2.1.3.1. 2-[2-(4-(4-Methylpiperidin-1-yl)benzylidene)hydrazinyl]-4-phenylthiazole (3a).

FTIR (ATR, cm^{-1}): υ_{max} 3292 (N—H), 3072 (aromatic C—H), 2924 (aliphatic C—H), 1600–1442 (C═N and C═C), 1132 (C—N). ^{1}H NMR (300 Mhz, DMSO-d_6, ppm) δ 0.92 (3H, d, J = 6.5 Hz, CH_3), 1.12–1.25 (2H, m, piperidine protons), 1.49–1.58 (1H, m, piperidine proton), 1.67 (2H, d, J = 12.7 Hz, piperidine protons), 2.72 (2H, d, J = 11.4 Hz, piperidine protons), 3.77 (2H, d, J = 12.6 Hz, piperidine protons), 6.95 (2H, d, J = 8.9 Hz, aromatic protons), 7.26 (1H, s, aromatic proton), 7.30 (1H, d, J = 7.2 Hz, aromatic proton), 7.40 (2H, t, J = 7.7 Hz, aromatic protons), 7.47 (2H, d, J = 8.8 Hz, aromatic protons), 7.85 (2H, d, J = 7.2 Hz, aromatic protons), 7.91 (1H, s, CH═N), 11.89 (1H, s, NH). ^{13}C NMR (75 MHz, DMSO-d_6, ppm) δ 22.23 (CH_3), 30.70, 33.71, 48.40, 103.52, 115.36, 124.21, 125.95, 127.92, 129.03, 135.26, 142.37, 152.16, 168.84. HRMS (m/z): $[M+H]^+$ calcd for $C_{22}H_{24}N_4S$: 377.1794; found 377.1782.

2.1.3.2. 2-[2-(4-(4-Methylpiperidin-1-yl)benzylidene)hydrazinyl]-4-(4-methylphenyl)thiazole (3b).

FTIR (ATR, cm^{-1}): υ_{max} 3296 (N—H), 3091 (aromatic C—H), 2918 (aliphatic C—H), 1600–1516 (C═N and C═C), 1224 (C—N). ^{1}H NMR (300 Mhz, DMSO-d_6, ppm) δ 0.92 (3H, d, J = 6.5 Hz, CH_3), 1.12–1.27 (2H, m, piperidine protons), 1.51–1.62 (1H, m, piperidine proton), 1.69 (2H, d, J = 12.6 Hz, piperidine protons), 2.31 (3H, s, CH_3), 2.73–2.93 (2H, m, piperidine protons), 3.76 (2H, d, J = 12.6 Hz, piperidine protons), 6.98–7.05 (2H, m, aromatic protons), 7.18–7.21 (3H, m, aromatic protons), 7.48 (2H, d, J = 8.7 Hz, aromatic protons), 7.73 (2H, d, J = 8.1 Hz, aromatic protons), 7.91 (1H, s, CH═N), 11.87 (1H, s, NH). ^{13}C NMR (75 MHz, DMSO-d_6, ppm) δ 21.26 (CH_3), 22.18 (CH_3), 30.54, 33.61, 47.48, 48.72, 102.65, 114.21, 115.63, 125.91, 127.92, 129.60, 132.59, 137.15, 142.18, 150.95, 154.12, 168.72. HRMS (m/z): $[M+H]^+$ calcd for $C_{23}H_{26}N_4S$: 391.1951; found 391.1940.

2.1.3.3. 2-[2-(4-(4-Methylpiperidin-1-yl)benzylidene)hydrazinyl]-4-(4-bromophenyl)thiazole (3c).

FTIR (ATR, cm^{-1}): υ_{max} 3387 (N—H), 3074 (aromatic C—H), 2949 (aliphatic C—H), 1602–1440 (C═N and C═C), 1049 (C—N). ^{1}H NMR (300 Mhz, DMSO-d_6, ppm) δ 0.97 (3H, d, J = 6.5 Hz, CH_3), 1.45–1.49 (1H, m, piperidine proton), 1.71–1.91 (4H, m, piperidine protons), 3.26 (2H, br s, piperidine protons), 3.67 (2H, d, J = 11.9 Hz, piperidine protons), 7.41–7.53 (3H, m, aromatic protons), 7.60 (2H, d, J = 8.6 Hz, aromatic protons), 7.69–7.71 (2H, m, aromatic protons), 7.80 (2H, d, J = 8.5 Hz, aromatic protons), 8.02 (1H, s, CH═N), 12.22 (1H, s, NH). ^{13}C NMR (75 MHz, DMSO-d_6, ppm) δ 21.70 (CH_3), 28.86, 32.41, 47.72, 48.12, 105.05, 121.01, 128.02, 129.19, 129.87, 132.01, 134.25, 137.36, 142.67, 150.97, 154.94, 168.73. HRMS (m/z): $[M+H]^+$ calcd for $C_{22}H_{23}BrN_4S$: 455.0900; found 455.0886.

2.1.3.4. 2-[2-(4-(4-Methylpiperidin-1-yl)benzylidene)hydrazinyl]-4-(4-chlorophenyl)thiazole (3d).

FTIR (ATR, cm^{-1}): υ_{max} 3298 (N—H), 3087 (aromatic C—H), 2918 (aliphatic C—H), 1602–1462 (C═N and C═C), 1226 (C—N). ^{1}H NMR (300 Mhz, DMSO-d_6, ppm) δ 0.92 (3H, d, J = 6.5 Hz, CH_3), 1.12–1.26 (2H, m, piperidine protons), 1.49–1.61 (1H, m, piperidine proton), 1.68 (2H, d, J = 12.4 Hz, piperidine protons), 2.73 (2H, t, J = 10.5 Hz, piperidine protons), 3.78 (2H, d, J = 12.7 Hz, piperidine protons), 6.96 (2H, d, J = 8.9 Hz, aromatic protons), 7.34 (1H, s, aromatic proton), 7.44–7.48 (4H, m, aromatic protons), 7.86 (2H, d, J = 8.6 Hz, aromatic protons), 7.91 (1H, s, CH═N), 11.89 (1H, s, NH). ^{13}C NMR (75 MHz, DMSO-d_6, ppm) δ 22.23 (CH_3), 30.69, 33.69, 48.41, 104.37, 115.38, 127.66, 127.96, 129.05, 132.27, 134.12, 142.55, 168.97. HRMS (m/z): $[M+H]^+$ calcd for $C_{22}H_{23}ClN_4S$: 411.1405; found 411.1388.

2.1.3.5. 2-[2-(4-(4-Methylpiperidin-1-yl)benzylidene)hydrazinyl]-4-(4-fluorophenyl)thiazole (3e).

FTIR (ATR, cm^{-1}): υ_{max} 3298 (N—H), 3111 (aromatic C—H), 2918 (aliphatic C—H), 1600–1516 (C═N and C═C), 1222 (C—N). ^{1}H NMR (300 Mhz, DMSO-d_6, ppm) δ 0.92 (3H, d, J = 6.5 Hz, CH_3), 1.12–1.25 (2H, m, piperidine protons), 1.49–1.59 (1H, m, piperidine proton), 1.67 (2H, d, J = 12.6 Hz, piperidine

protons), 2.72 (2H, td, J_1 = 2.2 Hz, J_2 = 12.3 Hz, piperidine protons), 3.77 (2H, d, J = 12.7 Hz, piperidine protons), 6.95 (2H, d, J = 8.9 Hz, aromatic protons), 7.20–7.25 (3H, m, aromatic protons), 7.46 (2H, d, J = 8.9 Hz, aromatic protons), 7.85–7.91 (3H, m, aromatic protons, CH═N), 11.88 (1H, s, NH). ^{13}C NMR (75 MHz, DMSO-d_6, ppm) δ 22.23 (CH_3), 30.70, 33.70, 48.39, 103.28, 115.36, 115.86 (d, J = 21 Hz), 124.18, 127.90 (d, J = 7.5 Hz), 131.92, 142.47, 152.17, 162.00 (d, J = 242.3 Hz), 168.94. HRMS (m/z): $[M + H]^+$ calcd for $C_{22}H_{23}FN_4S$: 395.1700; found 395.1692.

*2.1.3.6. 2-[2-(4-(4-Methylpiperidin-1-yl)benzylidene)hydrazinyl]-4-(4-nitrophenyl)thiazole (**3f**).* FTIR (ATR, cm^{-1}): υ_{max} 3309 (N−H), 3034 (aromatic C−H), 2922 (aliphatic C−H), 1597–1566 (C═N and C═C), 1514–1336 (NO_2), 1224 (C−N). ^{1}H NMR (300 Mhz, DMSO-d_6, ppm) δ 0.92 (3H, d, J = 6.5 Hz, CH_3), 1.16–1.27 (2H, m, piperidine protons), 1.52–1.58 (1H, m, piperidine proton), 1.70 (2H, d, J = 12.3 Hz, piperidine protons), 2.79 (2H, br s, piperidine protons), 3.77 (2H, d, J = 12.6 Hz, piperidine protons), 7.01 (2H, d, J = 6.2 Hz, aromatic protons), 7.50 (2H, d, J = 8.5 Hz, aromatic protons), 7.67 (1H, s, aromatic proton), 7.94 (1H, s, CH═N), 8.10 (2H, d, J = 9 Hz, aromatic protons), 8.27 (2H, d, J = 9 Hz, aromatic protons), 12.04 (1H, s, NH). ^{13}C NMR (75 MHz, DMSO-d_6, ppm) δ 22.16 (CH_3), 30.49, 33.56, 48.82, 108.57, 115.62, 124.57, 126.76, 128.05, 141.23, 142.76, 146.61, 148.95, 169.22. HRMS (m/z): $[M + H]^+$ calcd for $C_{22}H_{23}N_5O_2S$: 422.1645; found 422.1636.

*2.1.3.7. 2-[2-(4-(4-Methylpiperidin-1-yl)benzylidene)hydrazinyl]-4-(4-cyanophenyl)thiazole (**3 g**).* FTIR (ATR, cm^{-1}): υ_{max} 3248 (N−H), 3105 (aromatic C−H), 2968 (aliphatic C−H), 2223 (C≡N), 1602–1514 (C═N and C═C), 1226 (C−N). ^{1}H NMR (300 Mhz, DMSO-d_6, ppm) δ 0.91 (3H, d, J = 6.5 Hz, CH_3), 1.11–1.25 (2H, m, piperidine protons), 1.49–1.58 (1H, m, piperidine proton), 1.67 (2H, d, J = 12.7 Hz, piperidine protons), 2.72 (2H, td, J_1 = 2.1 Hz, J_2 = 12.4 Hz, piperidine protons), 3.77 (2H, d, J = 12.7 Hz, piperidine protons), 6.95 (2H, d, J = 8.9 Hz, aromatic protons), 7.47 (2H, d, J = 8.8 Hz, aromatic protons), 7.58 (1H, s, aromatic proton), 7.86 (2H, d, J = 8.5 Hz, aromatic protons), 7.93 (1H, s, CH═N), 8.02 (2H, d, J = 8.5 Hz, aromatic protons), 11.96 (1H, s, NH). ^{13}C NMR (75 MHz, DMSO-d_6, ppm) δ 22.23 (CH_3), 30.70, 33.70, 48.35, 107.47, 109.94, 115.32, 119.48, 124.01, 126.54, 128.02, 133.13, 139.36, 142.84, 149.27, 152.24, 169.15. HRMS (m/z): $[M+H]^+$ calcd for $C_{23}H_{23}N_5S$: 402.174; found 402.1735.

*2.1.3.8. 2-[2-(4-(4-Methylpiperidin-1-yl)benzylidene)hydrazinyl]-4-(4-hydroxyphenyl)thiazole (**3 h**).* FTIR (ATR, cm^{-1}): υ_{max} 3329 (N−H), 3068 (aromatic C−H), 2918 (aliphatic C−H), 1600–1514 (C═N and C═C), 1226–1047 (C−N and C−O). ^{1}H NMR (300 Mhz, DMSO-d_6, ppm) δ 0.91 (3H, d, J = 6.5 Hz, CH_3), 1.14–1.25 (2H, m, piperidine protons), 1.57–1.70 (3H, m, piperidine protons), 2.83–2.92 (2H, m, piperidine protons), 3.60–3.74 (2H, m, piperidine protons), 6.78 (2H, d, J = 8.7 Hz, aromatic protons), 6.96–7.15 (3H, m, aromatic protons), 7.46–7.53 (2H, m, aromatic protons), 7.64 (2H, d, J = 8.7 Hz, aromatic protons), 7.93 (1H, s, CH═N), 9.57 (1H, s, OH), 11.89 (1H, s, NH). ^{13}C NMR (75 MHz, DMSO-d_6, ppm) δ 22.08 (CH_3), 30.76, 33.31, 47.56, 100.62, 114.30, 115.73, 116.81, 127.36, 127.90, 129.32, 129.62, 131.76, 133.34, 157.70, 164.31. HRMS (m/z): $[M+H]^+$ calcd for $C_{22}H_{24}N_4OS$: 393.1744; found 393.1738.

*2.1.3.9. 2-[2-(4-(4-Methylpiperidin-1-yl)benzylidene)hydrazinyl]-4-(2,4-difluorophenyl)thiazole (**3i**).* FTIR (ATR, cm^{-1}): υ_{max} 3290 (N−H), 3130 (aromatic C−H), 2951 (aliphatic C−H), 1600–1487 (C═N and C═C), 1136 (C−N). ^{1}H NMR (300 Mhz, DMSO-d_6, ppm) δ 0.92 (3H, d, J = 6.5 Hz, CH_3), 1.12–1.25 (2H, m, piperidine protons), 1.48–1.60 (1H, m, piperidine proton), 1.68 (2H, d, J = 12.6 Hz, piperidine protons), 2.73 (2H, t, J = 11.9 Hz, piperidine protons), 3.77 (2H, d, J = 12.7 Hz, piperidine protons), 6.96 (2H, d, J = 8.8 Hz, aromatic protons), 7.14–7.20 (2H, m, aromatic protons), 7.30–7.38 (1H, m, aromatic protons), 7.47 (2H, d, J = 8.8 Hz, aromatic protons), 7.92 (1H, s, CH═N), 7.98–8.06 (1H, m, aromatic protons), 11.91 (1H, s, NH). ^{13}C NMR (75 MHz, DMSO-d_6, ppm) δ 22.22 (CH_3), 30.68, 33.68, 48.41, 104.98, 107.59, 107.78, 112.14, 112.42, 115.38, 127.98, 130.83, 142.63, 152.14, 158.24, 161.74, 163.15, 168.31. HRMS (m/z): $[M+H]^+$ calcd for $C_{22}H_{22}F_2N_4S$: 413.1606; found 413.1604.

*2.1.3.10. 2-[2-(4-(4-Methylpiperidin-1-yl)benzylidene)hydrazinyl]-4-(3,4-hydroxyphenyl)thiazole (**3j**).* FTIR (ATR, cm^{-1}): υ_{max} 3263 (N−H), 3059 (aromatic C−H), 2974 (aliphatic C−H), 1620–1487 (C═N and C═C), 1265–1082 (C−N and C−O). ^{1}H NMR (300 Mhz, DMSO-d_6, ppm) δ 0.93 (3H, d, J = 5.6 Hz, CH_3), 1.53–1.76 (5H, m, piperidine protons), 3.15 (1H, br s, piperidine proton), 3.50–3.60 (3H, m, piperidine protons), 6.41–6.50 (1H, m, aromatic proton), 6.74 (2H, d, J = 8.2 Hz, aromatic protons), 6.95–6.96 (1H, m, aromatic proton), 7.23–7.73 (5H, m, aromatic protons), 8.02 (1H, s, CH═N), 8.99 (2H, br s, OH), 12.22 (1H, s, NH). ^{13}C NMR (75 MHz, DMSO-d_6, ppm) δ 21.77 (CH_3), 29.19, 32.32, 47.72, 106.73, 115.63, 116.39, 117.51, 119.53, 120.72, 124.73, 127.94, 128.12, 129.12, 142.93, 145.63, 145.98, 152.43, 169.49. HRMS (m/z): $[M+H]^+$ calcd for $C_{22}H_{24}N_4O_2S$: 409.1693; found 409.1689.

*2.1.3.11. 2-[2-(4-(3-Methylpiperidin-1-yl)benzylidene)hydrazinyl]-4-phenylthiazole (**3k**).* FTIR (ATR, cm^{-1}): υ_{max} 3267 (N−H), 3091 (aromatic C−H), 2945 (aliphatic C−H), 1600–1442 (C═N and C═C), 1232 (C−N). ^{1}H NMR (300 Mhz, DMSO-d_6, ppm) δ 0.91 (3H, d, J = 6.5 Hz, CH_3), 1.00–1.13 (1H, m, piperidine proton), 1.46–1.69 (4H, m, piperidine protons), 2.40 (1H, t, J = 11.5 Hz, piperidine proton), 2.69 (1H, t, J = 10.2 Hz, piperidine proton), 3.71 (2H, t, J = 11.2 Hz, piperidine protons), 6.96 (2H, d, J = 8.6 Hz, aromatic protons), 7.27–7.31 (2H, m, aromatic protons), 7.40 (2H, t, J = 7.7 Hz, aromatic protons), 7.47 (2H, d, J = 8.8 Hz, aromatic protons), 7.85 (2H, d, J = 8.5 Hz, aromatic protons), 7.91 (1H, s, CH═N), 11.89 (1H, s, NH). ^{13}C NMR (75 MHz, DMSO-d_6, ppm) δ 19.68 (CH_3), 24.88, 30.52, 32.93, 48.53, 56.02, 103.54, 115.35, 125.95, 127.95, 129.03, 135.26, 142.37, 168.83. HRMS (m/z): $[M + H]^+$ calcd for $C_{22}H_{24}N_4S$: 377.1794; found 377.1781.

*2.1.3.12. 2-[2-(4-(3-Methylpiperidin-1-yl)benzylidene)hydrazinyl]-4-(4-methylphenyl)thiazole (**3l**).* FTIR (ATR, cm^{-1}): υ_{max} 3238 (N−H), 3047 (aromatic C−H), 2987 (aliphatic C−H), 1600–1442 (C═N and C═C), 1234 (C−N). ^{1}H NMR (300 Mhz, DMSO-d_6, ppm) δ 0.91 (3H, d, J = 6.5 Hz, CH_3), 1.03–1.15 (1H, m, piperidine proton), 1.54–1.76 (4H, m, piperidine protons), 2.26–2.42 (4H, m, piperidine protons, CH_3), 2.71–2.73 (1H, m, piperidine proton), 2.56–2.73 (2H, m, piperidine protons), 6.96–7.06 (3H, m, aromatic protons), 7.19 (3H, t, J = 8.4 Hz, aromatic protons), 7.40–7.51 (2H, m, aromatic protons), 7.73 (1H, d, J = 8.1 Hz, aromatic proton), 7.91 (1H, s, CH═N), 11.89 (1H, s, NH). ^{13}C NMR (75 MHz, DMSO-d_6, ppm) δ 19.61 (CH_3), 21.28 (CH_3), 24.76, 30.48, 32.73, 47.41, 48.76, 102.68, 114.08, 115.66, 125.91, 127.95, 128.17, 129.23, 129.60, 132.05, 137.17, 142.12, 150.06, 154.58, 168.91. HRMS (m/z): $[M+H]^+$ calcd for $C_{23}H_{26}N_4S$: 391.1951; found 391.1946.

*2.1.3.13. 2-[2-(4-(3-Methylpiperidin-1-yl)benzylidene)hydrazinyl]-4-(4-bromophenyl)thiazole (**3m**).* FTIR (ATR, cm^{-1}): υ_{max} 3338 (N−H), 3076 (aromatic C−H), 2974 (aliphatic C−H), 1600–1458 (C═N and C═C), 1234 (C−N). ^{1}H NMR (300 Mhz, DMSO-d_6, ppm) δ 0.93 (3H, d, J = 6.5 Hz, CH_3), 1.03–1.15 (1H, m, piperidine proton), 1.54–1.79 (4H, m, piperidine protons), 2.79–2.97 (1H, m, piperidine proton), 3.63–3.95 (3H, m, piperidine protons), 7.03–7.43 (6H, m, aromatic protons), 7.59 (2H, d, J = 8.6 Hz, aromatic protons), 7.80 (1H, d, J = 8.5 Hz, aromatic proton), 7.97 (1H, s, CH═N), 12.13 (1H, s, NH). ^{13}C NMR (75 MHz, DMSO-d_6, ppm) δ 19.45 (CH_3), 30.28, 34.62, 46.72, 48.37, 103.72, 114.81, 115.37, 125.82, 127.31, 128.01, 130.26,

131.99, 137.92, 142.73, 151.34, 154.82, 168.19. HRMS (*m/z*): [M + H]$^+$ calcd for $C_{22}H_{23}BrN_4S$: 455.0900; found 455.0885.

*2.1.3.14. 2-[2-(4-(3-Methylpiperidin-1-yl)benzylidene)hydrazinyl]-4-(4-chlorophenyl)thiazole (**3n**).* FTIR (ATR, cm^{-1}): υ_{max} 3381 (N—H), 3078 (aromatic C—H), 2974 (aliphatic C—H), 1602–1438 (C═N and C═C), 1234 (C—N). ^{1}H NMR (300 Mhz, DMSO-d_6, ppm) δ 0.92 (3H, d, J = 6.5 Hz, CH_3), 1.05–1.13 (1H, m, piperidine proton), 1.59–1.75 (4H, m, piperidine protons), 2.80 (1H, br s, piperidine proton), 3.65–3.76 (3H, m, piperidine protons), 7.03–7.27 (4H, m, aromatic protons), 7.36 (1H, s, aromatic proton), 7.44–7.55 (3H, m, aromatic protons), 7.86 (1H, d, J = 8.6 Hz, aromatic proton), 7.95 (1H, s, CH═N), 12.00 (1H, s, NH). ^{13}C NMR (75 MHz, DMSO-d_6, ppm) δ 19.53 (CH_3), 24.63, 30.38, 33.46, 48.73, 104.41, 115.99, 127.67, 128.01, 129.07, 129.96, 132.92, 134.92, 142.46, 168.37. HRMS (*m/z*): [M + H]$^+$ calcd for $C_{22}H_{23}ClN_4S$: 411.1405; found 411.1395.

*2.1.3.15. 2-[2-(4-(3-Methylpiperidin-1-yl)benzylidene)hydrazinyl]-4-(4-fluorophenyl)thiazole (**3o**).* FTIR (ATR, cm^{-1}): υ_{max} 3338 (N—H), 3070 (aromatic C—H), 2945 (aliphatic C—H), 1602–1438 (C═N and C═C), 1232 (C—N). ^{1}H NMR (300 Mhz, DMSO-d_6, ppm) δ 0.92 (3H, d, J = 6.5 Hz, CH_3), 1.00–1.14 (1H, m, piperidine proton), 1.54–1.77 (4H, m, piperidine protons), 2.70 (1H, br s, piperidine proton), 3.56–3.73 (3H, m, piperidine protons), 6.96–7.07 (3H, m, aromatic protons), 7.20–7.32 (3H, m, aromatic protons), 7.43–7.50 (2H, m, aromatic protons), 7.86–7.92 (2H, m, aromatic proton, CH═N), 11.91 (1H, s, NH). ^{13}C NMR (75 MHz, DMSO-d_6, ppm) δ 19.59 (CH_3), 24.75, 30.45, 32.77, 56.23, 103.33, 114.06, 115.38, 115.68 (d, J = 3.2 Hz), 115.99, 127.86, 127.97, 128.92, 130.26 (d, J = 8 Hz), 131.77, 132.13, 142.34, 161.88 (d, J = 243.7 Hz), 163.34, 166.52, 168.93. HRMS (*m/z*): [M + H]$^+$ calcd for $C_{22}H_{23}FN_4S$: 395.1700; found 395.1687.

*2.1.3.16. 2-[2-(4-(3-Methylpiperidin-1-yl)benzylidene)hydrazinyl]-4-(4-nitrophenyl)thiazole (**3p**).* FTIR (ATR, cm^{-1}): υ_{max} 3346 (N—H), 3080 (aromatic C—H), 2904 (aliphatic C—H), 1597–1446 (C═N and C═C), 1508–1338 (NO_2), 1107 (C—N). ^{1}H NMR (300 Mhz, DMSO-d_6, ppm) δ 0.93 (3H, d, J = 6.5 Hz, CH_3), 1.12–1.21 (1H, m, piperidine proton), 1.69–1.82 (4H, m, piperidine protons), 2.78–2.99 (1H, m, piperidine proton), 3.63 (1H, t, J = 12.8 Hz, piperidine proton), 4.49 (2H, br s, piperidine protons), 7.11–7.14 (1H, m, aromatic proton), 7.43–7.51 (2H, m, aromatic protons), 7.63–7.73 (2H, m, aromatic protons), 7.85–8.12 (3H, m, CH═N, aromatic protons), 8.22–8.29 (2H, m, aromatic protons), 12.30 (1H, s, NH). ^{13}C NMR (75 MHz, DMSO-d_6, ppm) δ 19.19 (CH_3), 30.02, 31.25, 32.90, 48.27, 108.73, 113.27, 124.60, 126.81, 128.11, 129.50, 146.67, 169.02. HRMS (*m/z*): [M + H]$^+$ calcd for $C_{22}H_{23}N_5O_2S$: 422.1645; found 422.1637.

*2.1.3.17. 2-[2-(4-(3-Methylpiperidin-1-yl)benzylidene)hydrazinyl]-4-(4-cyanophenyl)thiazole (**3q**).* FTIR (ATR, cm^{-1}): υ_{max} 3298 (N—H), 3080 (aromatic C—H), 2958 (aliphatic C—H), 2484 (C≡N), 1602–1512 (C═N and C═C), 1147 (C—N). ^{1}H NMR (300 Mhz, DMSO-d_6, ppm) δ 0.93 (3H, d, J = 6.5 Hz, CH_3), 1.18–1.24 (1H, m, piperidine proton), 1.78–1.97 (4H, m, piperidine protons), 2.96–3.22 (2H, m, piperidine protons), 3.57–3.65 (2H, m, piperidine protons), 7.37–7.55 (3H, m, aromatic protons), 7.65–7.73 (3H, m, aromatic protons), 7.87 (2H, d, J = 8.6 Hz, aromatic protons), 8.03 (2H, d, J = 8.3 Hz, CH═N, aromatic proton), 12.30 (1H, s, NH). ^{13}C NMR (75 MHz, DMSO-d_6, ppm) δ 19.14 (CH_3), 23.82, 29.93, 48.72, 108.08, 110.06, 119.45, 126.58, 128.09, 133.18, 139.16, 141.17, 149.27, 168.90. HRMS (*m/z*): [M + H]$^+$ calcd for $C_{23}H_{23}N_5S$: 402.1747; found 402.1738.

*2.1.3.18. 2-[2-(4-(3-Methylpiperidin-1-yl)benzylidene)hydrazinyl]-4-(4-hydroxyphenyl)thiazole (**3r**).* FTIR (ATR, cm^{-1}): υ_{max} 3267 (N—H), 3126 (aromatic C—H), 2951 (aliphatic C—H), 1571–1512 (C═N and C═C), 1141 (C—N). ^{1}H NMR (300 Mhz, DMSO-d_6, ppm) δ 0.93 (3H, d, J = 6.5 Hz, CH_3), 1.16 (1H, br s, piperidine proton), 1.78–1.81 (4H, m, piperidine protons), 2.84–3.11 (2H, m, piperidine protons), 3.60–3.68 (2H, m, piperidine protons), 6.61–6.84 (2H, m, aromatic protons), 7.04 (1H, s, aromatic proton), 7.33–7.44 (2H, m, aromatic protons), 7.65 (4H, d, J = 8.6 Hz, aromatic protons), 8.01 (1H, s, CH═N), 9.59 (1H, s, OH), 12.18 (1H, s, NH). ^{13}C NMR (75 MHz, DMSO-d_6, ppm) δ 19.25 (CH_3), 23.22, 30.08, 34.04, 48.71, 101.07, 115.75, 126.08, 127.44, 128.06, 129.91, 132.72, 134.64, 142.72, 157.63, 168.43. HRMS (*m/z*): [M + H]$^+$ calcd for $C_{22}H_{24}N_4OS$: 393.1744; found 393.1737.

*2.1.3.19. 2-[2-(4-(3-Methylpiperidin-1-yl)benzylidene)hydrazinyl]-4-(2,4-difluorophenyl)thiazole (**3s**).* FTIR (ATR, cm^{-1}): υ_{max} 3273 (N—H), 3049 (aromatic C—H), 2924 (aliphatic C—H), 1595–1485 (C═N and C═C), 1261 (C—N). ^{1}H NMR (300 Mhz, DMSO-d_6, ppm) δ 0.91 (3H, d, J = 6.6 Hz, CH_3), 1.04–1.12 (1H, m, piperidine proton), 1.50–1.79 (4H, m, piperidine protons), 2.35–2.43 (1H, m, piperidine proton), 2.64–2.75 (1H, m, piperidine proton), 3.68–3.79 (2H, m, piperidine protons), 6.94–7.01 (2H, m, aromatic protons), 7.14–7.20 (2H, m, aromatic protons), 7.30–7.38 (1H, m, aromatic proton), 7.47 (1H, d, J = 8.9 Hz, aromatic proton), 7.65 (1H, d, J = 8.3 Hz, aromatic proton), 7.92 (1H, s, CH═N), 7.98–8.06 (1H, m, aromatic proton), 11.90 (1H, s, NH). ^{13}C NMR (75 MHz, DMSO-d_6, ppm) δ 19.68 (CH_3), 24.88, 30.53, 32.97, 48.44, 55.91, 104.98, 107.68 (d, J = 13.3 Hz), 112.25 (d, J = 21.7 Hz), 114.43, 115.27, 128.00, 130.83, 142.67, 152.21, 158.40, 168.30. HRMS (*m/z*): [M + H]$^+$ calcd for $C_{22}H_{22}F_2N_4S$: 413.1606; found 413.1600.

*2.1.3.20. 2-[2-(4-(3-Methylpiperidin-1-yl)benzylidene)hydrazinyl]-4-(3,4-hydroxyphenyl)thiazole (**3t**).* FTIR (ATR, cm^{-1}): υ_{max} 3238 (N—H), 3122 (aromatic C—H), 2953 (aliphatic C—H), 1595–1485 (C═N and C═C), 1263 (C—N). ^{1}H NMR (300 Mhz, DMSO-d_6, ppm) δ 0.91 (3H, d, J = 6.3 Hz, CH_3), 1.11–1.20 (1H, m, piperidine proton), 1.74–2.18 (4H, m, piperidine protons), 2.78–3.08 (2H, m, piperidine protons), 3.51–3.55 (2H, m, piperidine protons), 6.42–6.51 (1H, m, aromatic proton), 6.95 (1H, s, aromatic proton), 7.10–7.43 (3H, m, aromatic protons), 7.59–7.72 (3H, m, aromatic proton), 8.02 (1H, s, CH═N), 9.02 (2H, br s, OH), 12.47 (1H, s, NH). ^{13}C NMR (75 MHz, DMSO-d_6, ppm) δ 19.27 (CH_3), 29.85, 33.18, 48.19, 106.18, 115.63, 116.41, 119.50, 121.18, 124.86, 127.86, 128.16, 129.46, 142.72, 145.62, 145.97, 152.38, 169.87. HRMS (*m/z*): [M + H]$^+$ calcd for $C_{22}H_{24}N_4O_2S$: 409.1693; found 409.1687.

2.2. MAO inhibition assay

The fluorometric enzyme inhibition assay was carried out to investigate the inhibition profiles of the synthesized compounds as in previously defined by us [29,30]. Ampliflu™ Red (10-Acetyl-3,7-dihydroxyphenoxazine) was used as fluorescence reagent in this assay. All reagents and enzymes (Ampliflu™ Red, peroxidase from horseradish, *h*MAO-A, *h*MAO-B, H_2O_2, tyramine hydrochloride, moclobemide and selegiline) were supplied from Sigma-Aldrich (Steinheim, Germany).

In the enzymatic assay, three different daily prepared solutions were used. (I) Inhibitor solutions: Synthesized compounds and reference agents were prepared in 2% DMSO in 10^{-3}–10^{-9} M concentrations (10 mL for each concentration). (II) Enzyme solutions: Recombinant *h*MAO-A (0.5 U/mL) and recombinant *h*MAO-B (0.64 U/mL) enzymes were dissolved in the phosphate buffer and final volumes were adjusted to 10 mL. (III) Working solution: Horseradish peroxidase (200 U/mL, 100 µL), Ampliflu™ Red (20 mM, 200 µL) and tyramine (100 mM, 200 µL) were dissolved in the phosphate buffer and final volume was adjusted to 10 mL.

The solutions of inhibitor (20 µL/well) and *h*MAO-A (100 µL/well) or *h*MAO-B (100 µL/well) were added to the flat black bottom 96-well micro test plate, and incubated at 37 °C for 30 min. After this incubation period, the reaction was started by adding a working solution (100 µL/well). The mixture was incubated at 37 °C for 30 min and the fluorescence (Ex/Em = 535/587 nm) was measured at 5 min intervals. Control

experiments were carried out simultaneously by replacing the inhibitor solution with 2% DMSO (20 µL). To check the probable inhibitory effect of inhibitors on horseradish peroxidase, a parallel reading was performed by replacing enzyme solutions with %3 H_2O_2 solution (20 mM 100 µL/well). In addition, the possible capacity of the inhibitors to modify the fluorescence generated in the reaction mixture due to non-enzymatic inhibition was determined by mixing inhibitor and working solutions.

The specific fluorescence emission (used to obtain the final results) was calculated after subtraction of the background activity, which was determined from vials containing all components except the *h*MAO isoforms, which were replaced by phosphate buffer (100 µL/well). Blank, control and all concentrations of inhibitors were analyzed in quadruplicate and inhibition percent was calculated by using following equation:

$$\%\text{Inhibition} = \frac{(FC_{t2} - FC_{t1}) - (FI_{t2} - FI_{t1})}{FC_{t2} - FC_{t1}} \times 100$$

where FCt_2: Fluorescence of a control well measured at t_2 time, FCt_1: Fluorescence of a control well measured at t_1 time, FIt_2: Fluorescence of an inhibitor well measured at t_2 time, FIt_1: Fluorescence of an inhibitor well measured at t_1 time. The IC_{50} values were calculated from a dose-response curve obtained by plotting the percentage inhibition versus the log concentration with the use of Microsoft Office Excel 2013. The results were displayed as mean ± standard deviation (SD).

2.3. Enzyme kinetic studies

Enzyme kinetic studies were performed for compounds **3j** and **3 t** in order to determine the inhibition type on MAO enzymes. The same materials were used in the MAO inhibition assay. The most active compounds **3j** and **3t** were tested at three different concentrations (IC_{50}/2, IC_{50} and 2 × IC_{50}). The solutions of inhibitor (20 µL/well) and enzyme were added to the flat black bottom 96-well micro test plate, and incubated at 37 °C for 30 min. After incubation period, the working solution, including various concentrations (20, 10, 5, 2.5, 1.25, and 0.625 µM) of tyramine (100 µL/well) was added. The increase of the fluorescence (Ex/Em = 535/587 nm) was recorded for 30 min. A parallel experiment was carried out without inhibitor. All processes were assayed in quadruplicate. The results were analyzed as Lineweaver-Burk plots using Microsoft Office Excel 2013. The K_m / V_{max} (slope) values of the Lineweaver-Burk plots were replotted versus the inhibitor concentration, and the K_i values were determined from the x-axis intercept as -K_i.

2.4. Cytotoxicity test

MTT test was performed to determine the cytotoxic profile of the most active compounds **3j** and **3t** using the NIH/3T3 mouse embryonic fibroblast cell line (ATCC® CRL-1658™, London, UK). The method was executed in the same way as we have reported in our previous work [31].

2.5. Theoretical determination of ADME properties

ADME parameters of all synthesized compounds were assessed with the help of *QikProp 4.8* software [32].

2.6. Molecular docking studies

In order to determine the binding modes of compounds **3j** and **3 t** on *h*MAO-A and *h*MAO-B enzyme active site, docking studies were performed. X-ray crystal structures of *h*MAO-A (PDB ID: 2Z5X) [33] and *h*MAO-B (PDB ID: 2V5Z) [34] were retrieved from the Protein Data Bank (www.pdb.org).

The structures of ligands were built using the *Schrödinger Maestro* [35] interface and then were submitted to the *Protein Preparation Wizard* protocol of the *Schrödinger Suite 2016 Update 2* [36]. The ligands were prepared by the *LigPrep 3.8* [37] to assign the protonation states at pH 7.4 ± 1.0 and the atom types, correctly. Bond orders were assigned and hydrogen atoms were added to the structures. The grid generation was formed using *Glide 7.1* [38]. The grid box with dimensions of 20 Å × 20 Å × 20 Å was centered in the vicinity of the flavin (FAD) N5 atom on the catalytic site of the protein to cover all binding sites and neighboring residues [39–41]. Flexible docking runs were performed with single precision docking mode (SP).

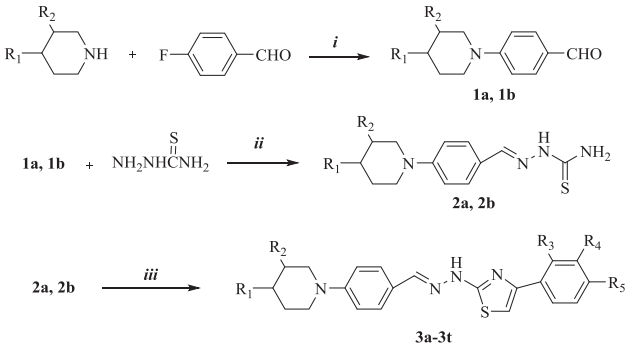

Scheme 1. Synthesis of the compounds (**3a**-**3t**). Reactants, reagents, and conditions; (***i***) K_2CO_3, DMF, reflux, 24 h; (***ii***) EtOH, reflux, 4 h; (***iii***) appropriate phenacyl bromides, EtOH, reflux, 3 h.

3. Results and discussion

3.1. Chemistry

The title compounds (**3a-3t**) were obtained according the multi-step strategy outlined in Scheme 1. Reaction of 3 or 4-substituted piperidine with 4-fluorobenzaldehyde resulted in the formation of 4-substituted benzaldehyde derivatives (**1a, 1b**) which were then treated with thiosemicarbazide to afford the corresponding thiosemicarbazones (**2a, 2b**). Subsequently, the intramolecular cyclization of compounds (**2a, 2b**) with appropriate phenacyl bromide derivatives generated the target thiazole compounds (**3a-3 t**) in good yields. Some properties of the compounds were presented in Table 1.

The structural elucidation of the final compounds was performed by FT-IR ^{1}H NMR, ^{13}C NMR, and HRMS. In the IR spectra, characteristic stretching bands noted at between 3387 and 3238 cm^{-1}, 1620–1438 cm^{-1}, 1263–1049 cm^{-1} belong to N—H, C═N and C═C, C—N bonds, respectively.

In the ^{1}H NMR spectra, methyl protons linked to piperidine were observed at about 0.92–0.97 ppm as doublet peak. Azomethine (—CH═N) and N—H protons were recorded as singlet peaks at the region of 7.91–8.03 ppm and 11.87–12.47 ppm, respectively. Aromatic protons were assigned in range 6.41–8.29 ppm. In the ^{13}C NMR spectra, peaks at about 19.14–22.23 ppm were recorded for methyl carbons attached to piperidine. Aromatic carbons were generally detected at 100.62–169.87 ppm range. Molecular ion peaks were designated in agreement with molecular weights of the compounds.

3.2. MAO inhibition assay

The fluorometric method was applied in two steps in order to investigate the *h*MAO-A and *h*MAO-B isoenzymes inhibitory activity of all synthesized compounds (**3a**-**3t**). Final compounds were prepared and tested at the initial concentrations (10^{-3} and 10^{-4} M) in the first step. According to the first step results, the compounds showing > 50% inhibition were selected for the second stage. In this second step, 10^{-5}–10^{-9} M concentrations of the selected compounds were prepared and used. Considering Table 2, only compounds **3a, 3b, 3k,** and **3l**

Table 1
Some properties of the synthesized compounds (**3a-3t**).

Compound	R_1	R_2	R_3	R_4	R_5	Yield (%)	M.p. (°C)	Molecular formula	Molecular weight
3a	CH_3	H	H	H	H	75	187	$C_{22}H_{24}N_4S$	376,52
3b	CH_3	H	H	H	CH_3	70	230	$C_{23}H_{26}N_4S$	390,55
3c	CH_3	H	H	H	Br	68	209	$C_{22}H_{23}BrN_4S$	455,42
3d	CH_3	H	H	H	Cl	70	182	$C_{22}H_{23}ClN_4S$	410,96
3e	CH_3	H	H	H	F	69	165	$C_{22}H_{23}FN_4S$	394,51
3f	CH_3	H	H	H	NO_2	71	205	$C_{22}H_{23}N_5O_2S$	421,52
3g	CH_3	H	H	H	CN	70	217	$C_{23}H_{23}N_5S$	401,53
3h	CH_3	H	H	H	OH	70	170	$C_{22}H_{24}N_4OS$	392,52
3i	CH_3	H	F	H	F	76	175	$C_{22}H_{22}F_2N_4S$	412,50
3j	CH_3	H	H	OH	OH	67	233	$C_{22}H_{24}N_4O_2S$	408,52
3k	H	CH_3	H	H	H	72	150	$C_{22}H_{24}N_4S$	376,52
3l	H	CH_3	H	H	CH_3	75	120	$C_{23}H_{26}N_4S$	390,55
3m	H	CH_3	H	H	Br	67	157	$C_{22}H_{23}BrN_4S$	455,42
3n	H	CH_3	H	H	Cl	65	157	$C_{22}H_{23}ClN_4S$	410,96
3o	H	CH_3	H	H	F	68	146	$C_{22}H_{23}FN_4S$	394,51
3p	H	CH_3	H	H	NO_2	60	183	$C_{22}H_{23}N_5O_2S$	421,52
3q	H	CH_3	H	H	CN	65	216	$C_{23}H_{23}N_5S$	401,53
3r	H	CH_3	H	H	OH	69	235	$C_{22}H_{24}N_4OS$	392,52
3s	H	CH_3	F	H	F	71	155	$C_{22}H_{22}F_2N_4S$	412,50
3t	H	CH_3	H	OH	OH	73	209	$C_{22}H_{24}N_4O_2S$	408,52

Table 2
% Inhibition of compounds **3a-3t**, moclobemide and selegiline at the initial concentrations against MAO-A and MAO-B.

Compound	MAO-A IC_{50} (μM)	MAO-B IC_{50} (μM)	*SI	Selectivity
3c	0.849 ± 0.023	0.665 ± 0.018	1,28	MAO-B
3d	0.452 ± 0.011	0.152 ± 0.005	2,97	MAO-B
3e	0.187 ± 0.012	0.117 ± 0.003	1,60	MAO-B
3f	0.594 ± 0.018	0.184 ± 0.007	3,23	MAO-B
3g	0.380 ± 0.014	0.137 ± 0.004	2,77	MAO-B
3h	0.280 ± 0.011	0.109 ± 0.003	2,57	MAO-B
3i	0.194 ± 0.022	0.184 ± 0.017	1,05	MAO-B
3j	0.134 ± 0.004	0.027 ± 0.001	4,96	MAO-B
3m	0.765 ± 0.028	0.698 ± 0.024	1,10	MAO-B
3n	0.442 ± 0.017	0.149 ± 0.004	2,97	MAO-B
3o	0.202 ± 0.011	0.114 ± 0.003	1,77	MAO-B
3p	0.524 ± 0.020	0.173 ± 0.006	3,03	MAO-B
3q	0.338 ± 0.013	0.136 ± 0.005	2,49	MAO-B
3r	0.277 ± 0.010	0.104 ± 0.003	2,66	MAO-B
3s	0.209 ± 0.016	0.196 ± 0.022	1,07	MAO-B
3t	0.123 ± 0.005	0.025 ± 0.001	4,92	MAO-B
Moclobemide	6.054 ± 0.173	–	–	MAO-A
Selegiline	–	0.039 ± 0.001	–	MAO-B

* The selectivity index (SI) was calculated as IC_{50} (MAO-A) / IC_{50} (MAO-B).

could not pass the second step of *h*MAO-A and hMAO-B enzymes inhibition assay. The IC_{50} values of compounds against *h*MAO-A and *h*MAO-B enzymes are given in Table 2. Compounds **3j** and **3t** showed IC_{50} values of 0.134 ± 0.004 μM and 0.123 ± 0.005 μM, respectively, whereas standard drug moclobemide had an IC_{50} of 6.054 ± 0.173 μM on *h*MAO-A. In *h*MAO-B inhibition study, compounds **3j** and **3t** were the most active derivatives with IC_{50} values of 0.027 ± 0.001 μM and 0.025 ± 0.001 μM. Selegiline was used as a reference drug in *h*MAO-B enzyme activity and showed an IC_{50} of 0.039 ± 0.001 μM.

Selectivity indexes (SI), calculated as IC_{50}(MAO-A)/IC_{50}(MAO-B), are presented in Table 2. SI < 1 means selectivity towards MAO-A, while SI > 1 shows selectivity towards MAO-B. The data in Table 2 shows that synthesized compounds possess selectivity towards MAO-B. However, very close SIs to 1 suggests that enzyme selectivity is not evident.

In terms of SARs the phenyl group at C4 of the thiazole is the structural property that should be evaluated first. Because, significant changes in enzyme inhibition have been observed by the alterations of substituent type and position on phenyl group. It has been reported that ortho and/or para substitution of phenyl group are responsible for enzyme inhibition [20,21]. Interestingly, in the present study non-substitution and para methyl substitution of phenyl group caused a dramatic activity loss. On the other hand, all other compounds, bearing halogen, hydroxyl, nitro or cyano substituents, displayed moderate to good inhibition against both isoenzymes. According to biological activity results, compounds **3j** and **3t** were found as the most active derivatives in the series against both MAO isoenzymes. When these compounds are structurally examined, it can be seen that their substitution pattern is different from those of compounds reported both in our previous [28] and present studies. Both **3j** and **3t** carry hydroxyl groups at meta and para positions of phenyl ring. Thus, it can be suggested that 3,4-dihydroxy substitution has an important influence on both *h*MAO-A and *h*MAO-B enzyme inhibition.

The N1 of hydrazine moiety is another important region of the compounds for an intrinsic enzyme inhibition. According to literature N1 of the hydrazine group has steric and electronic influences on enzyme-inhibitor interaction [20,21]. From this knowledge in the present study we incorporated 4-(3- or 4-methylpiperidin-1-yl)benzylidene fragment to N1 of hydrazine. Although 3- or 4-methyl substitutions of piperidine do not cause different inhibition potencies each other, they have a great contribution on the enzyme inhibition potency of the compounds compared with the compounds that we reported previously [28].

3.3. Enzyme kinetic studies

MAO inhibitors are divided into two types as reversible or irreversible inhibitors. The first produced MAO inhibitors inhibit based on mechanism and they bind to proteins covalently. These irreversible inhibitors have serious side effects like hallucination, schizophrenia and hypertension. They perform covalent binding to the proteins to yield reactive products. In addition to these kinds of MAO inhibitors also had noticeable hepatotoxic side effects, by inactivating the P450, which cannot be tolerated. Therefore, for newly developed drug candidates, reversible inhibition types as uncompetitive, competitive, non-competitive, or mixed type are required in order to avoid such side effects.

The enzyme kinetic studies of compounds **3j** and **3t** on both *h*MAO-A and *h*MAO-B enzymes were carried out in order to determine the inhibition type and thus predict whether or not they have the side effects mentioned above. Kinetic studies were applied with a similar procedure to the MAO inhibition assay. The type of inhibition was specified with the help of Lineweaver-Burk graphics [42]. Enzyme kinetics were examined by recording substrate velocity curves in the absence and presence of the most effective compounds **3j** and **3t**, which

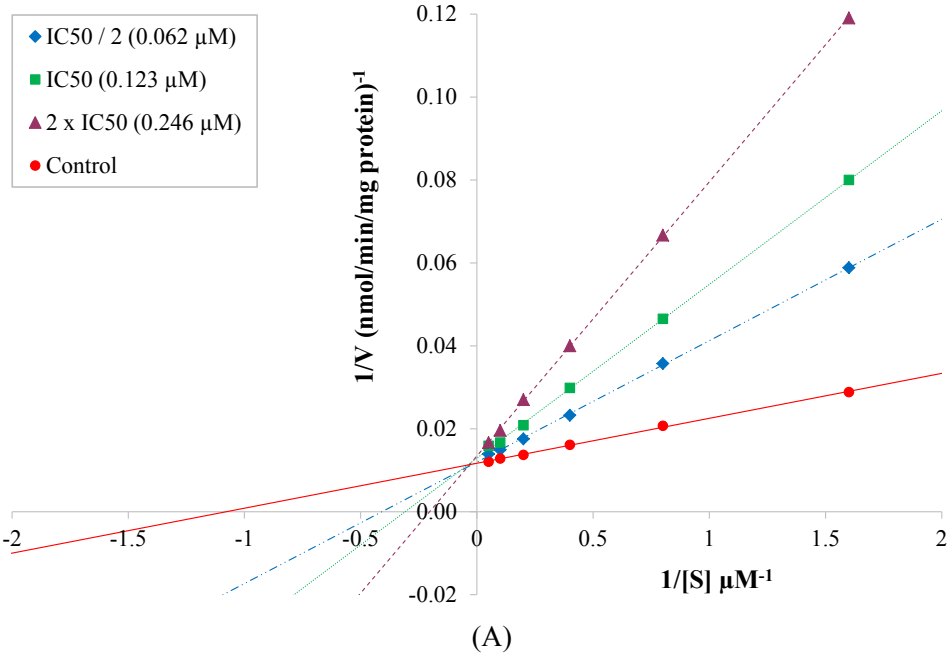

(A)

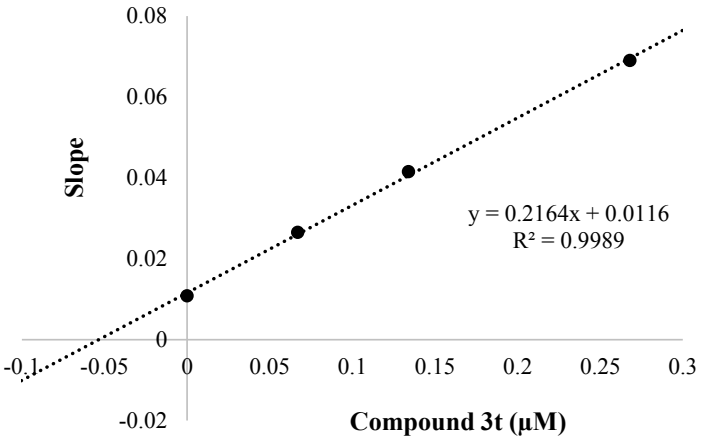

(B)

Fig. 2. (A) Lineweaver–Burk plots for the inhibition of *h*MAO-A by compound **3 t**. [S], substrate concentration (µM); V, reaction velocity (nmol/min/mg protein). Inhibitor concentrations are shown at the left. K_m values from 2 × IC_{50} to Control; 5.111, 3.192, 2.208 and 0.923 (µM). V_{max} value of the competitive inhibition; 79.950 ± 2.341 (nmol/min/mg protein). **(B)** Secondary plot for calculation of steady-state inhibition constant (K_i) of compound **3t**. K_i was calculated as 0.054 µM.

were prepared at 2xIC_{50}, IC_{50} and IC_{50}/2 concentrations. The substrate (tyramine) was used at different concentrations ranging from 0.625 µM to 20 µM, and thus the initial velocity measurements were obtained. Then, Dixon plots were formed by using the data gained from Lineweaver-Burk graphics in order to calculate K_i values of compounds **3j** and **3t**. The graphical analysis of steady-state inhibition data are presented for **3t** in Figs. 2 and 3 and given for **3j** in **Supporting Information Figs. S1 and S2**.

In the Lineweaver-Burk graphics of compounds **3j** and **3 t**, intersection of plots on y-axis and different slopes and intercepts on x-axis describe the competitive inhibition type. Hence, it can be stated that these compounds are reversible and competitive inhibitors against *h*MAO-A and *h*MAO-B enzymes, so have similar inhibition features with the substrate. The K_i values for compounds **3j** and **3t** were calculated as 0.071 µM and 0.052 µM, respectively, for the inhibition of *h*MAO-A, whereas their K_i values on *h*MAO-B enzyme kinetics were found as 0.012 µM and 0.010 µM, respectively.

3.4. Cytotoxicity test

As a general medicinal chemistry approach a drug candidate should also not be toxic in addition to its essential biological activity. Therefore, the most active derivatives **3j** and **3t** were screened for their cytotoxicity profiles. Thus, MTT assay was applied by using healthy NIH/3T3 mouse embryonic fibroblast cell line (ATCC CRL1658), which is recommended for cytotoxicity screening by ISO (10993-5, 2009) [43]. It can be seen from Table 3, compounds **3j** and **3t** had IC_{50} values of > 1000 µM and 600 µM, respectively, against NIH/3T3 cells. These IC_{50} values are very higher than those obtained in MAO-B enzyme inhibition assay (0.027 µM and 0.025 µM, respectively). As a result, compounds **3j** and **3t** have been proven to be non-toxic in their effective concentration against *h*MAO-B.

3.5. Calculated ADME parameters

Having favorable ADME (absorption, distribution, metabolism, excretion) properties is one of the most challenging obstacles for drug

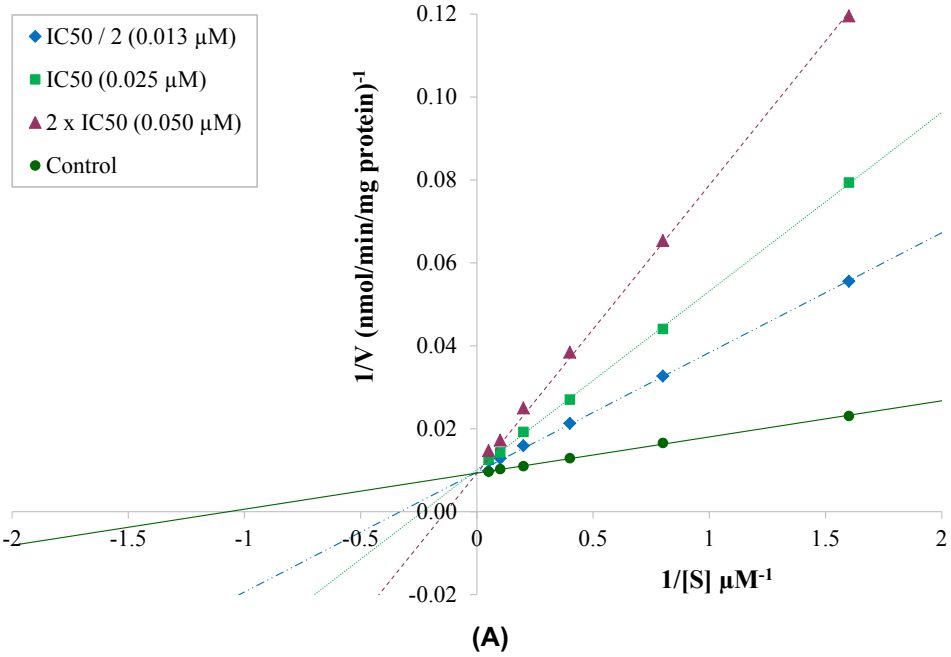

(A)

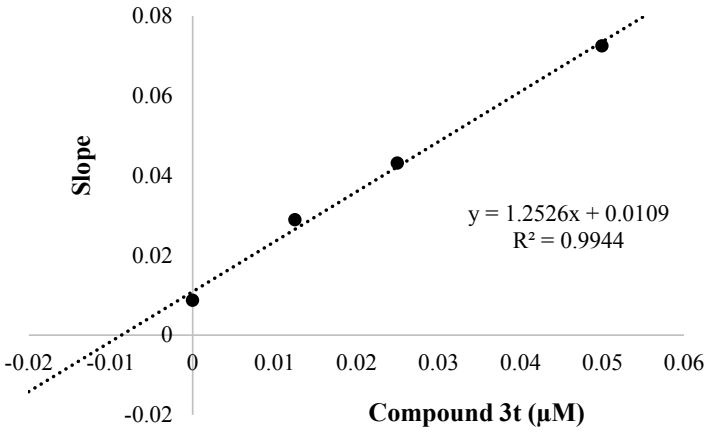

(B)

Fig. 3. (A) Lineweaver–Burk plots for the inhibition of *h*MAO-B by compound **3t**. [S], substrate concentration (µM); V, reaction velocity (nmol/min/mg protein). Inhibitor concentrations are shown at the left. K_m values from 2 × IC_{50} to Control; 7.796, 4.267, 3.042 and 0.935 (µM). V_{max} value of the competitive inhibition; 104.832 ± 2.023 (nmol/min/mg protein). **(B)** Secondary plot for calculation of steady-state inhibition constant (K_i) of compound **3t**. K_i was calculated as 0.010 µM.

Table 3
The IC_{50} value of the compounds **3j** and **3t** against NIH/3T3 cell line.

Compound	Cell Line	IC_{50}(µM)
3j	NIH/3T3	> 1000
3t	NIH/3T3	600

development. ADME expresses the properties of absorption, distribution, metabolism and excretion of a molecule within an organism. All these features are important for any drug. The early optimization could be provided by ADME calculation. Early resolution of problems that cause ADME failure prevents later time loss. Identification and elimination of adverse compounds make the research process more effective and efficient [44]. For this reason, to predict the pharmacokinetic properties of new drug candidates as early as possible in the drug development process is very important.

ADME predictions of all synthesized compounds (**3a-3t**) were carried out by *QikProp 4.8* software [32]. *QikProp* also provides acceptable ranges for comparing the predicted properties of compounds with those of 95% of known drugs. In addition to ADME properties, drug-likeness properties were also estimated by *QikProp*. The drug-likeness of a compounds was assessed according to Lipinski's Rule of Five [45], which considers molecular weight (< 500 Da), number of hydrogen bond acceptors (≤10) and donors (≤5), and octanol/water partition coefficient (≤5) and Jorgensen's rule of three [46], which regards logS (> -5.7), PCaco (> 22 nm/s), primary metabolites (PM) (< 7). These rules are essential for the optimization of biologically active compounds, and thus, they must not be violated.

The predicted ADME properties are presented in Table 4 and this table contains the following parameters: Molecular weight (MW), number of rotatable bonds (RB), dipole moment (DM), molecular volume (MV), number of hydrogen donors (DHB), number of hydrogen acceptors (AHB), polar surface area (PSA), octanol/water partition coefficient (log P), aqueous solubility (log S), apparent Caco-2 cell

Table 4
Calculated ADME parameters of compounds **3a-3t**.

Comp.	MW	RB	DM	MV	DHB	AHB	PSA	logP	logS	PCaco	logBB	PMDCK	PM	%HOA	VRF	VRT
3a	376.518	4	2.451	1276.917	1	5	40.192	5.606	−7.471	4525.096	0.051	4998.277	1	100	1	1
3b	390.545	4	1.975	1335.853	1	5	40.192	5.912	−8.040	4525.091	0.042	4998.272	2	100	1	1
3c	455.414	4	4.494	1329.949	1	5	40.194	6.179	−8.334	4524.991	0.232	10000.000	1	100	1	1
3d	410.963	4	4.810	1321.037	1	5	40.194	6.102	−8.217	4524.925	0.219	10000.000	1	100	1	1
3e	394.509	4	4.868	1293.032	1	5	40.196	5.842	−7.839	4524.816	0.163	9037.418	1	100	1	1
3f	421.516	5	12.450	1359.315	1	6	88.858	4.905	−7.716	465.090	−1.235	427.377	2	100	0	1
3g	401.528	5	8.783	1343.614	1	6.5	65.987	4.842	−8.418	935.800	−0.864	909.948	1	100	0	1
3h	392.518	5	2.720	1300.086	2	5.75	62.874	4.842	−7.158	1363.085	−0.638	1366.369	2	100	0	1
3i	412.499	4	4.004	1302.694	1	5	38.754	6.004	−8.068	4699.197	0.257	10000.000	1	100	1	1
3j	408.517	6	4.467	1321.534	3	6.5	84.384	4.125	−6.805	490.613	−1.241	452.783	3	100	0	1
3k	376.518	4	2.453	1276.949	1	5	40.192	5.606	−7.471	4525.096	0.051	4998.277	1	100	1	1
3l	390.545	4	1.977	1335.885	1	5	40.192	5.912	−8.039	4525.091	0.042	4998.272	2	100	1	1
3m	455.414	4	4.591	1322.774	1	5	38.829	6.132	−8.224	4524.991	0.235	10000.000	1	100	1	1
3n	410.963	4	4.908	1313.861	1	5	38.829	6.054	−8.108	4524.925	0.223	10000.000	1	100	1	1
3o	394.509	4	4.871	1293.064	1	5	40.196	5.842	−7.838	4524.816	0.163	9037.418	1	100	1	1
3p	421.516	5	12.555	1352.140	1	6	87.493	4.858	−7.608	465.090	−1.221	427.377	2	100	0	1
3q	401.528	5	8.885	1336.439	1	6.5	64.622	4.796	−8.310	935.800	−0.853	909.948	1	100	0	1
3r	392.518	5	2.730	1300.118	2	5.75	62.874	4.842	−7.158	1363.085	−0.637	1366.369	2	100	0	1
3s	412.499	4	4.122	1295.519	1	5	37.389	5.957	−7.959	4699.197	0.260	10000.000	1	100	1	1
3t	408.517	6	4.467	1321.566	3	6.5	84.384	4.126	−6.804	490.613	−1.241	452.783	3	100	0	1

MW: Molecular weight **RB:** Number of rotatable bonds **DM:** Computed dipole moment **MV:** Total solvent-accessible volume **DHB:** Estimated number of hydrogen bond donors **AHB:** Estimated number of hydrogen bond acceptors **PSA:** Van der Waals surface area of polar nitrogen and oxygen atoms and carbonyl carbon atoms **logP:** Predicted octanol/water partition coefficient **logS:** Predicted aqueous solubility **PCaco:** Predicted apparent Caco-2 cell permeability **logBB:** Predicted brain/blood partition coefficient **PMDCK:** Predicted apparent MDCK cell permeability **PM:** Number of likely metabolic reactions **%HOA:** Predicted human oral absorption percent **VRF:** Number of violations of Lipinski's rule of five. The rules are: MW < 500, logP < 5, DHB ≤ 5, AHB ≤ 10, Positive PSA value. **VRT:** Number of violations of Jorgensen's rule of three. The three rules are: logS > -5.7, PCaco > 22 nm/s, PM < 7.

permeability (PCaco), brain/blood partition coefficient (logBB), apparent MDCK cell permeability (PMDCK), number of likely primer metabolic reactions (PM), and percent of human oral absorption (% HOA), the violations of rules of three (VRT) and five (VRF). According to Lipinski's rule of five and Jorgensen's rule of three all compounds (**3a-3t**) are in accordance with the rule by causing no more than one violation.

Medicines targeted specifically to central nervous system should cross the blood-brain barrier (BBB). Thus, the ability to cross the blood brain barrier of these drugs of a great importance and should be evaluated in the early stage of drug development. For this purpose, apparent MDCK cell permeability (PMDCK) and brain/blood partition coefficient (logBB) were calculated. The MDCK cells are considered as a good mimic for the blood brain barrier. According to software predictions, the PMDCK values of < 25 and > 500 nm/s are recommended as poor and great for non-active transport of compound. So as to pass BBB, LogBB is another important parameter, which has recommended values of −3–1.2. According to Table 4, results of PMDCK and logBB are among these reference values and it can be said that all synthesized compounds are capable of crossing BBB.

As a consequence of ADME and BBB Permeability estimates, it can be suggested that the final compounds may have a good pharmacokinetic profile.

3.6. Molecular docking studies

Compounds **3j** and **3t** were found as the most active derivatives in the series as mentioned in MAO enzyme activity part. The common feature of these compounds is bearing dihydroxy moiety at 3rd and 4th positions of the phenyl ring. Therefore, the docking studies were conducted in order to determine *in silico* binding modes of these compounds and to be able to evaluate the contribution of the dihydroxy moiety to both MAO-A and MAO-B enzyme activities. The X-ray crystal structures of *h*MAO-A (PDB ID: 2Z5X) [33] and *h*MAO-B (PDB ID: 2V5Z) [34] were obtained from Protein Data Bank (www.pdb.org). The docking scores were calculated for all compounds. The obtained data (Table 5) confirmed the biological activity results. The most active compounds **3j** and **3t** also displayed the highest docking scores. The

Table 5
Docking scores of the compounds **3a-3t** against MAO-A and MAO-B enzymes.

Compound	MAO-A Docking Score (kcal/mol)	MAO-B Docking Score (kcal/mol)
3a	−9.749	−8.911
3b	−8.937	−9.247
3c	−7.692	−8.932
3d	−9.108	−9.143
3e	−9.732	−9.736
3f	−9.873	−8.375
3g	−7.641	−9.191
3h	−8.101	−9.454
3i	−9.866	−9.099
3j	−10.222	−10.354
3k	−8.821	−8.672
3l	−7.706	−7.619
3m	−7.849	−8.948
3n	−7.796	−9.015
3o	−8.67	−8.924
3p	−9.034	−8.076
3q	−9.423	−9.269
3r	−9.217	−9.417
3s	−9.116	−9.333
3t	−10.217	−10.079

docking poses of compounds are given in Figs. 4, 5 and in **Supporting information** (**Figs. S3-S12**).

The docking poses related to *h*MAO-A enzyme of compounds **3j** and **3t** are presented in Fig. 4**A, 5A, 5B** and in **Supporting information Figs. S3-S7.** Both compounds showed similar interactions. In compound **3j** the thiazole ring was in an interaction with phenyl of Tyr407 by doing π-π interaction, while for compound **3t**, this interaction was observed with phenyl of Tyr444. The N1 nitrogen of the hydrazine moiety emerged in terms of polar interaction. The N1 nitrogen formed a hydrogen bond with hydroxyl of Tyr444 in both compounds. The last interaction belonging to these compounds was a hydrogen bond, which was formed by hydroxyl moiety at the 3rd position of phenyl ring. In the compound **3j**, this hydroxyl group was in interaction with carbonyl of Arg51, while, hydroxyl moiety of compound **3t** created this interaction with amino of Lys305. These two compounds carry the hydroxyl

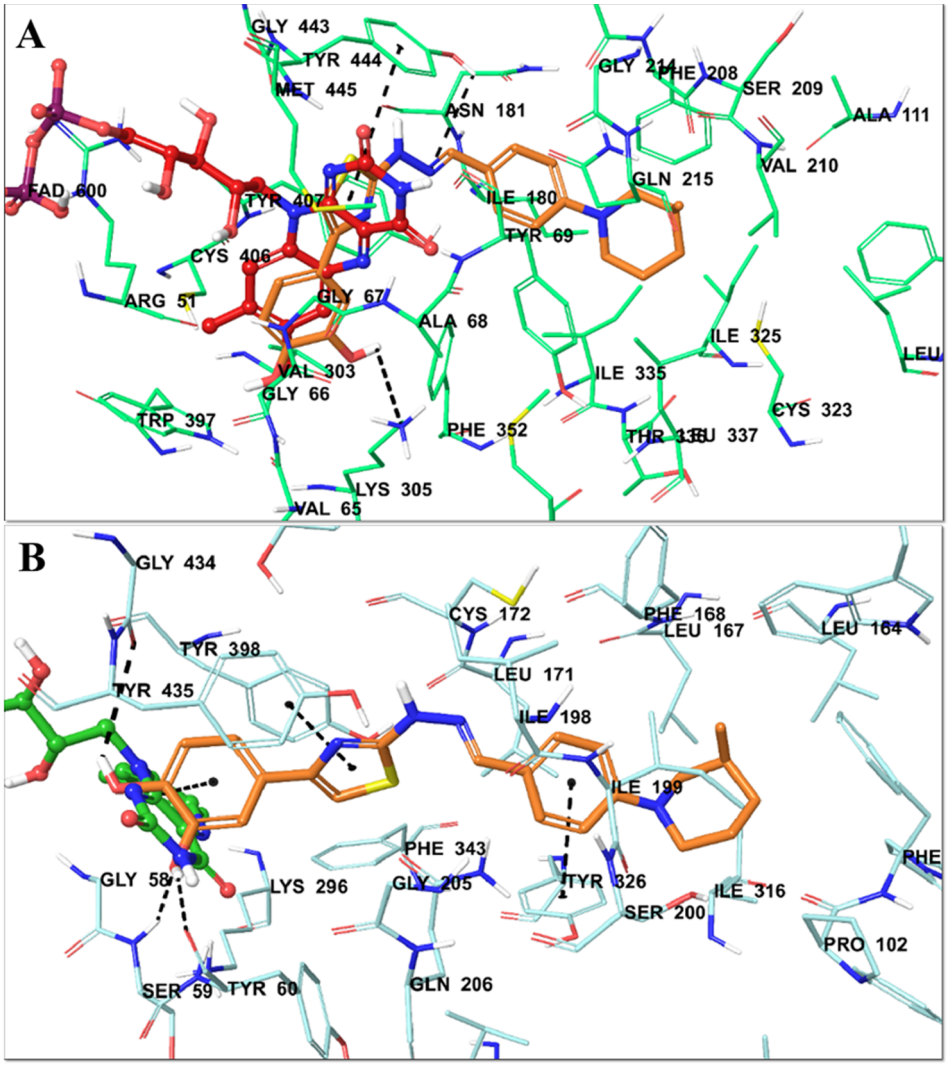

Fig. 4. A: The three-dimensional interacting modes of compound **3t** in the active region of *h*MAO-A. The inhibitor and the important residues in the active site of the enzyme are presented by tube model. The FAD molecule is coloured red with ball and stick model. **B:** The three-dimensional interacting modes of compound **3t** in the active region of *h*MAO-B. The inhibitor and the important residues in the active site of the enzyme are presented by tube model. The FAD molecule is coloured green with ball and stick model. (For interpretation of the references to colour in this figure legend, the reader is referred to the web version of this article.)

group at the 3rd position of the phenyl ring, unlike the remainder of the series. It can be suggested that owing to this additional interaction this position has a significant effect on the biological activity. The presence of a group capable of hydrogen bonding such as hydroxyl moiety at this position has a positive contribution on enzyme inhibition. All these findings explain the greater potency of compounds **3j** and **3t** on *h*MAO-A enzyme compared to the other compounds. Also, it can be seen from Fig. 5**A, B** and **Supporting information Figures S5, S6** that van der Waals and electrostatic interactions provide stronger binding to enzyme active site. Both compounds have favorable van der Waals interactions with Tyr60, Phe99, Phe103, Pro104, Trp119, Leu164, Leu167, Phe168, Leu171, Cys172, Ile198, Ser200, Gln206, Leu328, Tyr398 and Tyr435, displayed with pink and red colours as described in the user guide of *Glide* [38]. Especially, it is thought that piperidine and methyl moiety at its 4th position enhance van der Waals interaction with enzyme active region. These compounds also show promising electrostatic contributions with Phe103, Leu167, Leu171, Ile198, Tyr326 and Leu328.

Docking studies of compounds **3j** and **3t** against *h*MAO-B enzyme were also performed considering *h*MAO-A docking assays. The docking poses of *h*MAO-B are given in Fig. 4**B,** Fig. 5**C, D** and in **Supporting information Figs. S8-S12**. It can be understood from the docking poses that these compounds showed five identical interactions. The phenyl ring next to the piperidine was in an interaction with phenyl of Tyr326 by doing π-π interaction. The other π-π interaction was observed between thiazole ring and phenyl of Tyr398. In both compounds, dihydroxy substitution at 3rd and 4th positions of phenyl ring is very essential for polar interactions by doing three hydrogen bonds to bind enzyme active site. The hydroxy substituent at the 3rd position had two hydrogen bonds by interacting with amino of Ser59 acting as a hydrogen acceptor and carbonyl of Tyr60 acting as a hydrogen donor. The hydroxy moiety at the 4th position of phenyl formed another hydrogen bond with carbonyl of Gly434. This last hydrogen bond was observed in *h*MAO-B docking runs, unlike *h*MAO-A docking studies. Besides, van der Waals and electrostatic interactions of compounds **3j** and **3t** are presented in Fig. 5**C, D** and in **Supporting information Figs. S10, S11**. It can be seen that piperidine and methyl groups support binding to residues of enzyme active region by van der Waals interactions. Both compounds formed van der Waals interactions with Gly58, Ser59, Tyr60, Phe103, Trp119, Leu164, Leu167, Phe168, Leu171, Cys172, Ile198, Ile199, Gln206, Ile316, Tyr326, Phe343, Tyr398 and Tyr435, which were shown as pink and red colours [38]. Electrostatic interactions between docked compounds and Gly58, Ser59, Tyr60, Phe168, Gln206, Gly434 and Tyr435 were also observed.

All these findings explain more potent activity of compounds **3j** and

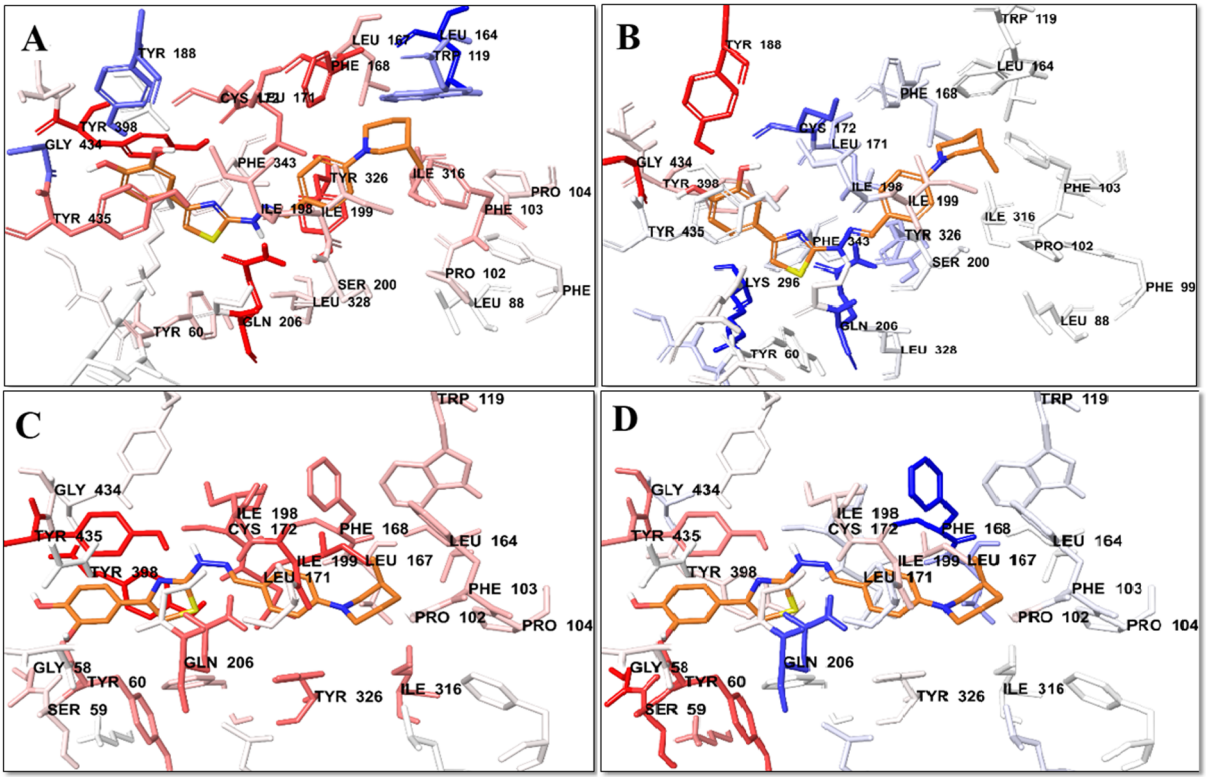

Fig. 5. A: The van der Waals interaction of compound **3t** with active region of *h*MAO-A. **B:** The electrostatic interaction of compound **3t** with active region of *h*MAO-A **C:** The van der Waals interaction of compound **3t** with active region of *h*MAO-B. **D:** The electrostatic interaction of compound **3t** with active region of *h*MAO-B. The residues displaying favourable van der Waals interactions have been shown with red and pink colour. The residues in electrostatic interaction are coloured with blue, red, and pink according to the distance from ligand by Per-Residue Interaction panel. (For interpretation of the references to colour in this figure legend, the reader is referred to the web version of this article.)

3t against *h*MAO-B enzyme. Furthermore, by looking at the general structure of the series, it can be suggested that both *h*MAO-A and *h*MAO-B inhibitions are positively affected by the presence of a hydroxy group, which is capable of a hydrogen bonding at the 3rd and 4th positions of phenyl ring.

4. Conclusion

In this study, our aim was to add new effective MAO compounds bearing thiazole ring to the literature. For this purpose, we have designed and synthesized new twenty thiazole derivatives and evaluated their *in vitro* and *in silico* biological activity against MAO isoenzymes. According to in vitro MAO enzyme inhibition assay results, compounds **3j** and **3t** were found as the most active derivatives in the series against both MAO-A and MAO-B enzymes. So as to clarify the inhibition type and *in silico* features of them, enzyme kinetic and docking studies were performed for these compounds. These compounds were assessed as reversible and competitive inhibitors of MAO-A and MAO-B enzymes. Also, it was indicated that these compounds were stronger than the other compounds in the series owing their different substituents. Furthermore, *in vitro* cytotoxicity and *in silico* ADME calculations have also shown that these compounds are promising MAO inhibitor candidates. Consequently, medicinal chemists may improve new molecules, which are more potent and safer MAO inhibitors, derived from compounds **3j** and **3t** for the treatment of neurological diseases based on these results.

Acknowledgment

his study was financially supported by Anadolu University Scientific Projects Fund, Project No: 1506S516.

Declaration of interest

The authors declare no conflicts of interest.

Appendix A. Supplementary material

Supplementary data to this article can be found online at https://doi.org/10.1016/j.bioorg.2018.12.019.

References

[1] C. Binda, A. Mattevi, D.E. Edmondson, Int. Rev. Neurobiol. 100 (2011) 1–11.
[2] M.B. Youdim, D. Edmondson, K.F. Tipton, Nat. Rev. Neurosci. 7 (4) (2006) 295–309.
[3] R.M. Geha, I. Rebrin, K. Chen, J.C. Shin, J. Biol. Chem. 276 (13) (2001) 9877–9882.
[4] L.J. Legobe, A. Petzer, J.P. Petzer, Bioorg. Chem. 45 (2012) 1–11.
[5] J. Wang, K. Huo, L. Ma, L. Tang, D. Li, X. Huang, Y. Yuan, C. Li, W. Wang, W. Guan, H. Chen, C. Jin, J. Wei, W. Zhang, Y. Yang, Q. Liu, Y. Zhou, C. Zhang, Z. Wu, W. Xu, Y. Zhang, T. Liu, D. Yu, Y. Zhang, L. Chen, D. Zhu, X. Zhong, L. Kang, X. Gan, X. Yu, Q. Ma, J. Yan, L. Zhou, Z. Liu, Y. Zhu, T. Zhou, F. He, X. Yang, Assoc. Mol. Syst. Biol. 536 (2011) 10–13.
[6] D.E. Edmondson, C. Binda, J. Wang, A.K. Upadhyay, A. Mattevi, Biochemistry 48 (2009) 4220–4230.
[7] N. Kaludercic, A. Carpi, R. Menabò, F. Di Lisa, N. Paolocci, Biochim. Biophys. Acta (BBA)-Mol. Cell Res. 1813 (7) (2011) 1323–1332.
[8] F. Chimenti, D. Secci, A. Bolasco, P. Chimenti, A. Granese, S. Carradori, O. Befani, P. Turini, S. Alcaro, F. Ortuso, Bioorg. Med. Chem. Lett. 16 (2006) 4135–4140.
[9] A.M. Helguera, A. Pérez-Garrido, A. Gaspar, J. Reis, F. Cagide, D. Vina, M.N. Cordeiro, F. Borges, Eur. J. Med. Chem. 59 (2013) 75–90.
[10] D.S. Knudsen-Gerber, Consult. Pharm. 26 (2011) 48–51.
[11] W.J. Geldenhuys, M.O. Funk, C.J. Van der Schyf, R.T. Carroll, Bioorg. Med. Chem. Lett. 22 (3) (2012) 1380–1383.
[12] R. Singh, S.N. Geetanjali, Chem. Biol. Lett. 1 (2014) 33–39.
[13] R.H. Haung, R. Faulkner, J. Biol. Chem. 256 (1981) 9211–9215.
[14] R. Pignatello, S. Mazzone, F. Castelli, P. Mazzone, G. Raciti, G. Mazzone, Pharmazie 49 (4) (1994) 272–276.

[15] D.E. Edmondson, C. Binda, A. Mattevı, Biochem. and Biophy. 464 (2007) 269–276.
[16] M. Ebadi, S.K. Srinivasan, M.D. Baxi, Prog. Neurobiol. 48 (1) (1996) 1–19.
[17] D. Secci, A. Bolasco, S. Carradori, M. D'Ascenzio, R. Nescatelli, M. Yáñez, Eur. J. Med. Chem. 58 (2012) 405–417.
[18] G. Raciti, P. Mazzone, A. Raudino, G. Mazzone, A. Cambria, Bioorg. Med. Chem. 3 (1995) 1485–1491.
[19] S. Gritsch, S. Guccione, R. Hoffmann, A. Cambria, G. Raciti, T. Langer, J. Enzyme Inhib. 16 (2001) 199–215.
[20] M. D'Ascenzio, S. Carradori, D. Secci, L. Mannina, A.P. Sobolev, C. De Monte, R. Cirilli, M. Yáñez, S. Alcaro, F. Ortuso, Bioorg. Med. Chem. 22 (10) (2014) 2887–2895.
[21] M. D'Ascenzio, P. Chimenti, M.C. Gidaro, C. De Monte, D. De Vita, A. Granese, L. Scipione, R. Di Santo, G. Costa, S. Alcaro, M. Yáñez, S. Carradori, J. Enzyme Inhib. Med. Chem. 30 (6) (2015) 908–919.
[22] A. Cambria, A. Raudino, A. Geronikaki, G. Buemi, G. Raciti, P. Mazzone, S. Guccione, S. Ragusa, J. Enzyme Inhib. 14 (4) (1999) 307–321.
[23] F. Chimenti, D. Secci, A. Bolasco, P. Chimenti, A. Granese, S. Carradori, M. Yáñez, F. Orallo, M.L. Sanna, B. Gallinella, R. Cirilli, J. Med. Chem. 53 (17) (2010) 6516–6520.
[24] F. Chimenti, E. Maccioni, D. Secci, A. Bolasco, P. Chimenti, A. Granese, O. Befani, P. Turini, S. Alcaro, F. Ortuso, M.C. Cardia, S. Distinto, J. Med. Chem. 50 (4) (2007) 707–712.
[25] F. Chimenti, E. Maccioni, D. Secci, A. Bolasco, P. Chimenti, A. Granese, S. Carradori, S. Alcaro, F. Ortuso, M. Yáñez, F. Orallo, R. Cirilli, R. Ferretti, F. La Torre, J. Med. Chem. 51 (16) (2008) 4874–4880.
[26] F. Chimenti, D. Secci, A. Bolasco, P. Chimenti, A. Granese, S. Carradori, E. Maccioni, M.C. Cardia, M. Yáñez, F. Orallo, S. Alcaro, F. Ortuso, R. Cirilli, R. Ferretti, S. Distinto, J. Kirchmair, T. Langer, Bioorg. Med. Chem. 18 (14) (2010) 5063–5070.
[27] F. Chimenti, A. Bolasco, D. Secci, P. Chimenti, A. Granese, S. Carradori, M. Yáñez, F. Orallo, F. Ortuso, S. Alcaro, Bioorg. Med. Chem. 18 (15) (2010) 5715–5723.
[28] N.Ö. Can, D. Osmaniye, S. Levent, B.N. Sağlık, B. Korkut, Ö. Atlı, Y. Özkay, Z.A. Kaplancıklı, Eur. J. Med. Chem. 144 (2018) 68–81.
[29] Ö.D. Can, D. Osmaniye, Ü. Demir Özkay, B.N. Sağlık, S. Levent, S. Ilgın, M. Baysal, Y. Özkay, Z.A. Kaplancıklı, Eur. J. Med. Chem. 131 (2017) 92–106.
[30] N.Ö. Can, D. Osmaniye, S. Levent, B.N. Sağlık, B. İnci, S. Ilgın, Y. Özkay, Z.A. Kaplancıklı, Molecules 22 (8) (2017) 1381.
[31] Ü. Demir Özkay, Ö.D. Can, B.N. Sağlık, U. Acar Çevik, S. Levent, Y. Özkay, S. Ilgın, Ö. Atlı, Bioorg. Med. Chem. Lett. 26 (2016) 5387–5394.
[32] QikProp, Version 4.8, Schr€odinger, LLC, New York, NY, 2016.
[33] S.Y. Son, J. Ma, Y. Kondou, M. Yoshimura, E. Yamashita, T. Tsukihara, Proc. Natl. Acad. Sci. (PNAS) 105 (15) (2008) 5739–5744.
[34] C. Binda, J. Wang, L. Pisani, C. Caccia, A. Carotti, P. Salvati, D.E. Edmondson, A. Mattevi, J. Med. Chem. 50 (2007) 5848–5852.
[35] Maestro, version 10.6, Schrödinger, LLC, New York, NY (2016).
[36] Schrödinger, LLC, New York, NY (2016).
[37] LigPrep, version 3.8, Schrödinger, LLC, New York, NY (2016).
[38] Glide, version 7.1, Schrödinger, LLC, New York, NY (2016).
[39] M. Toprakçı, K. Yelekçi, Bioorg. Med. Chem. Lett. 15 (2005) 4438–4446.
[40] N. Gökhan-Kelekçi, Ö.Ö. Şimşek, A. Ercan, K. Yelekçi, Z.S. Şahin, Ş. Işık, G. Uçar, A.A. Bilgin, Bioorg. Med. Chem. 17 (2009) 6761–6772.
[41] B. Evranos-Aksöz, S. Yabanoğlu-Çiftçi, G. Uçar, K. Yelekçi, R. Ertan, Bioorg. Med. Chem. Lett. 24 (2014) 3278–3284.
[42] 1st ed., Elsevier, Burlington, MA, USA, 2011, pp. 47–58.
[43] International Organization for Standardization, Biological Evaluation of Medical Devices-part 5: Tests for in Vitro Cytotoxicity ISO-10993-5, third ed., 2009.
[44] H. Van de Waterbeemd, E. Gifford, Nat. Rev. Drug Discov. 2 (3) (2003) 192–204.
[45] C.A. Lipinski, F. Lombardo, B.W. Dominy, P.J. Feeney, Adv. Drug Deliv. Rev. 46 (2001) 3–26.
[46] W.L. Jorgensen, E.M. Duffy, Adv. Drug Deliv. Rev. 54 (3) (2002) 355–366.